FOURTH EUROPEAN ROTORCRAFT AND POWERED LIFT AIRCRAFT FORUM

Paper No. 6

ROTOR PREDICTION WITH DIFFERENT DOWNWASH MODELS

R. STRICKER, W. GRADL

Messerschmitt-Bölkow-Blohm GmbH
Munich, Germany

September 13 - 15, 1978

STRESA - ITALY

Associazione Italiana di Aeronautica ed Astronautica
Associatione Industrie Aerospaziali

ROTOR PREDICTION WITH DIFFERENT DOWNWASH MODELS +)

R. Stricker, W. Gradl

Messerschmitt-Bolköw-Blohm GmbH
Munich, Germany
P.O. Box 801140

Summary

Rotor induced velocities have to be calculated accurately, in order to predict rotor performance, structural limitations, vibrations, stability and acoustics.

Three typical rotor downwash models in use today are called to mind. The fast local momentum theory is based on blade element - momentum analysis and an empirical relation for forward flight; both developed by Glauert. Vortex-wake models may be used to obtain better results, when the wake is near to the rotor. For the vortex models, the blade is represented by a lifting line and the wake is simulated by meshes of trailing and shed vortex elements. A typical experimental-prescribed-wake model uses an experimental wake geometry taken from hovering flight measurements, but the method may also be applied to forward flight if the geometry is distorted according to the free stream velocity. A more adequate representation of the wake geometry in forward flight might be obtained from free-wake analysis, where the wake elements are allowed to convect in the velocity field they create, until they take up positions which are consistent with the velocity field they induce.

A semi-empirical downwash model which combines momentum theory with properties of a vortex-wake model is introduced. Local momentum theory is extended by a simple wake of ring-vortices to simulate wake contraction effects. Wake geometry is taken from experiments also used for prescribed-wake models. Tip losses are simulated by increase of induced velocities following Prandtl. For forward flight, the induced velocities at hovering flight are used as input for a special superpositioning principle derived from experiment. Therefore, tip vortex - blade interactions and other effects known from vortex models and experiments can also be simulated even for flight cases when the wake is near to the rotor.

Results are presented for rotor blade loads, some specific data of flight dynamics, vibrations and acoustic characteristics. Calculated blade loads of the fast semi-empirical model are nearly identical to those from the much more expensive vortex model in hovering flight. In the transition flight region, the results are very similar and agreement with measurements is good in contrast to results from local momentum theory. As shown by prediction of cyclic control moment and rotor phase angle, the local momentum theory gives proper results for rotor calculations at hover but not for the transition flight region, where the semi-empirical model is adequate, e.g. in predicting the lateral control angle. Prediction of rotor hub inplane oscillatory forces and moments in hover and transition flight also show the usefulness of the semi-empirical method. As the oscillatory stresses predicted by the local momentum theory increase steadily with increasing advance ratio μ, the semi-empirical model shows forces/moments first increasing then decreasing and then increasing again with progressing μ, whereby agreement with measurements is acceptable. Finally an example of rotor noise calculation is given for a descending helicopter, that is when the wake is near to the rotor. Calculated blade loads show typical tip vortex - blade interaction effects at the advancing and retreating blade. The predicted sound pressure level agrees well with measurements up to a frequency according to the azimuthwise step used in blade loads calculation.

+) Work sponsored by the Ministry of Defence of the Federal Republic of Germany

NOTATION

b	number of blades
C	coefficient
M	moment
m	mass
P	force
R	blade radius
r	blade radial coordinate
T	thrust
t	time
V	velocity
x,y,z,	rectangular coordinates
γ	rotor angle of attack
θ	blade angle of attack
μ	advance ratio
ρ	density
σ	solidity
ϕ	rotor inflow angle
ψ	rotor azimuth angle
Ω	rotor angular velocity

INDICES

G	Glauert
i	induced
ib	in board
L	lift
LMT	local momentum theory
O	overall
T	thrust
tip	blade tip
TL	tip losses
∞	infinity

1. INTRODUCTION

The flow around a helicopter blade is heavily affected by the rotor downwash, especially in hovering and transition flight. The calculation of the induced velocities with sufficient accuracy is therefore a basic necessity in order to predict rotor performance, structural limitations, vibrations, stability and acoustic characteristics.

Methods for determining rotor inflow were originally developed for propellers. Simple momentum theory, based on the assumption of a uniformly loaded actuator disc without tip losses, was refined by introduction of blade element - momentum theory (References 1 and 2), resulting in a better representation of the radial inflow distribution. Tip losses were calculated (Reference 3) taking into account the finite number of blades. For forward flight the rotor was regarded as an elliptically loaded wing to which lifting-line theory could be applied (Reference 1). The result was an empirical momentum formula and the trapezoidal downwash distribution, both of which are still heavily used nowadays. Modified actuator disc theories (References 4 to 6) were developed to predict the rotor inflow variation versus azimuth and radius in forward flight.

Following the early development of the simple actuator disc and blade element - momentum methods, emphasis was placed on vortex theory, where the improvements of the methods largely paralleled the progress in the development of high-speed computers. Besides simple theories, using vortex cylinders and 'rectangularizations' of the vortex wake (e.g. References 7 and 8), the undistorted wake from each blade is modelled by straight trailing and shed vortex elements (e.g. References 9 to 11). The constant vorticity of the elements varies in accordance with the variation of the blade bound circulation in the azimuth and radial directions. The geometry of the wake is defined by the rotational and translational velocities of the rotor in planes parallel to the tip path plane and by the mean flow velocity in the axial direction, leading to the term 'prescribed-classical-wake models'.

The realization that the sensitivity of blade inflow and associated airloading to wake distortions can be significant, led to 'prescribed-contracted-wake models'. The roll-up of the spiral wake was taken into account by truncating the mesh of trailing and shed vortex elements behind the blade, at a given wake azimuth, and by providing thereafter for two concentrated vortex filaments to represent a rolled-up tip vortex and root vortex (References 11 and 12). Wake contraction has been considered analytically by many authors (e.g. References 13 and 14), but initially experimental investigations employing model rotors and flow visualization techniques, resulted in a sufficient description of wake characteristics in hovering flight (Reference 15) and in the 'prescribed-empirical-wake models' (e.g. References 15 and 16). For the 'free-wake models'

(e.g. References 17 and 18), the vortex elements are allowed to convect in the velocity field they create. The iteration either starts with an initial distribution of the vortex wake, or a process similar to the start-up of a rotor in a free stream is set up. The vortex elements move until they take up positions which are consistent with the velocity field they induce. As might be expected, the computing time for such calculations is prodigious.

The primary objectives of this paper are

- to compare typical rotor downwash models, such as local momentum theory, prescribed-contracted-wake analysis, and a free-wake model,
- to present a simple semi-empirical model which is based on local momentum theory but promises results, especially in transition flight, similar to those calculated with more expensive vortex models, and
- to describe results from these models calculating blade loads and specific flight dynamic data, rotor vibrations and acoustic characteristics.

2. TYPICAL ROTOR DOWNWASH MODELS IN USE TODAY

Treating the helicopter rotor as an integrated aerodynamic/dynamic system, rotor downwash has to be calculated rapidly with sufficient accuracy. A basic theory is the local momentum model as shown in Figure 1. In hovering flight it is identical to the blade element - momentum theory of Glauert (References 1 and 2). The radial variation of inflow is found by neglecting contraction of the wake and considering the rotor disc to be divided into concentric ring-segments, according to the number of blades. The thrust produced by each ring-segment is determined by blade element theory. By equating it to the overall momentum change in the air flow through each ring-segment, and assuming that the inflow is constant over the element, the inflow can then be determined. For forward flight conditions the simple linear representation of the fore-aft variation of inflow over the rotor (provided by Glauert, Reference 1) is added to the result from blade element - momentum theory. In this form, the local momentum theory may be used to calculate rotor performance and stability as well as the first harmonics of structural stresses in hovering flight and for advance ratios greater than about 0.15 with sufficient accuracy at low computing costs.

To calculate higher harmonics of aerodynamic loads in the transition flight region as well, vortex-wake models are in use. As the computing times are nearly equal for rigid-wake and prescribed-wake analyses, models such as the experimental-prescribed-contracted-wake model shown in Figure 2 are preferred (References 11 and 16). The blade is represented by a lifting line and the wake is divided into an inboard section and the tip vortex. In

the near wake, meshes of trailed and shed vortices form the inboard section, whereas a bundle of trailing vortices forms the tip vortex. In the mid wake the shed vortices are omitted and in the far wake there are only two single tip and root vortices. Wake geometry is taken from experimental investigations of Landgrebe (Reference 15), Figure 2. The radial and axial coordinates $\overline{r}_{tip}$, $\overline{Z}_{tip}$ of the tip vortex and the axial coordinates $\overline{Z}_{ib}$, r=0; $\overline{Z}_{ib}$, r=1 of the plane of the inboard section are given as functions of rotor thrust C_T, solidity σ, blade twist θ_v, number of blades b, and wake azimuth angle ψ. Though this wake geometry was evaluated only for hovering flight, it can also be used for forward flight, if the geometry is distorted according to the free stream velocity.

A more adequate representation of the wake geometry in forward flight might be obtained by using free-wake analysis such as the free-wake model of Sadler, see Figure 3 and Reference 18. The blade is again represented by a lifting line and the wake is calculated by a process similar to the start-up of a rotor in a free stream. An array of discrete trailing and shed vortices is generated with vortex strengths corresponding to stepwise radial and azimuth blade circulations. The array of shed and trailing vortices is limited to the near wake whereas an arbitrary number of trailing vortices form the far wake. The end points of the vortex elements are allowed to be transported by the resultant velocity of the free stream and vortex-induced velocities. Calculation is terminated when the vortices trailing from the blade during the first azimuthwise step no longer influence points of interest near the rotor disc. The results are wake geometry and wake flow data in addition to wake influence coefficients that may be used to calculate blade loads and blade response.

From the theoretical point of view, the three downwash models described above should satisfy the rotor designer's needs, but in standard rotor calculation of rotor performance, structural limitations, vibrations, stability, acoustics etc., the fast local momentum theory often gives poor results in the higher harmonics. Also computing time for vortex models, not to mention that for free-wake analysis, is excessive. Therefore, a semi-empirical downwash model, based on blade element-momentum theory and on an idea from Wood and Hermes (Reference 6) for induced flow build-up in forward flight, will be described below. The model might be an efficient tool for standard rotor calculations, especially in the transition flight region, both in terms of computing time and accuracy.

3. A SEMI-EMPIRICAL DOWNWASH MODEL

As shown in Reference 19 and Figure 4, the build-up of the induced velocities of a hovering rotor, following a rapid collective pitch increase of 200 deg./sec., will take about 1.2 sec. The curve of the induced velocities versus time may be approximated by an empirical relationship. From blade element - momentum theory, e.g. the induced velocity $V_{i(r,t\infty)}$ versus blade radius r at a time $t = \infty$,, is known. So the local induced velocity $V_{i(r,t)}$ for $t < \infty$ can be read from the start-up approximation. The local downwash may then be calculated by summing up the portions ΔV_1, ΔV_2,.... Of course, the result in hovering flight is identical to the value from blade element - momentum theory.

Transferring these relationships to forward flight, the build-up of the local induced velocities can be seen from Figure 5 for a blade at an azimuth angle of 180 deg., i.e. in flight direction for simplicity. In region A there is no induced velocity. Region B is affected by the induced velocity ΔV_1 that was built up during the time interval $\Delta t = 2 \cdot \pi / \Omega \cdot b$ by the preceding blade. For region C, the induced velocities ΔV_1 from the preceding blade and ΔV_2 from the pre-preceding blade have to be added. The induced velocity at region D however, is calculated by summing up the portions ΔV_1, ΔV_2 and ΔV_3, all calculated in accordance with their time intervals and the start-up approximation shown in Figure 4.

For a given blade element P (r,ψ) at any radial station r and azimuth station ψ we have to sum up the induced velocity portions ΔV_i, from all blades that have passed this point before. The azimuth angle ψ_{i+1} of the actual preceding blade may be calculated from an implicit equation. The time interval Δt_{i+1} depends on rotor angular velocity Ω, blade number b and blade azimuth angles ψ_i and ψ_{i+1} as shown in Figure 5. ΔV_i has to be calculated from the start-up approximation using Δt_{i+1} and the local induced velocity $V_{i(r_{i+1},\ \psi_{i+1})}$ for $t = \infty$ from blade element - momentum analysis as input. Summation of $\Delta V_i, \Delta V_{i+1}$... is terminated when the terms of the sum become small, either because the start-up approximation reaches the final value, or r_{i+1} becomes greater than the rotor radius, at which station V_i from blade element - momentum theory vanishes.

Local momentum theory, see Figure 1, is used as the basic inflow model to calculate the V_i at $t = \infty$. However, in the momentum equation of Glauert, the inplane component of the free stream velocity is omitted in order to calculate quasi-hovering cases in

forward flight, see Figure 6. This is done because the empirical momentum equation of Glauert for forward flight (Reference 1) is replaced by the empirical principle of superpositioning, shown in Figures 4 and 5.

Wake contraction is simulated by a wake of up to 4 ring vortices, see Figure 6, where the wake geometry is taken from the experimental-prescribed-contracted wake model of Landgrebe, see Reference 15 and Figure 2. The vorticity of the wake is calculated in accordance with the maximum blade circulation.

Tip losses are simulated by an increase of induced velocity V_{iTL} to produce a given thrust, see Figure 6. Following Prandtl (see Reference 20), V_{iTL} may be calculated from the number of blades b, radial station x, and inflow angle ϕ. Then the induced velocity portions, from modified blade element - momentum theory, from wake contraction simulation and from tip loss calculation, when added, will give the local induced velocity.

A block diagram for the rotor calculation using the semi-empirical downwash model is given in Figure 7. Input data are flight conditions and rotor data. Under the rotor trim loop and blade dynamics iteration loop, the rotor calculation is performed. Computation of induced velocity for a blade element is done under consideration of local momentum, forward speed superposition, and the influence of wake contraction and tip losses. The blade radial loop is followed by recalculation of the wake vorticity at the actual azimuth angle, and the rotor azimuth loop terminates the rotor calculation. Results are the rotor forces and moments, blade motion and loads, as well as rotor inflow and wake data.

4. RESULTS AND DISCUSSION

Comparison of computing times for the downwash models presented, is shown in Figure 8. Local momentum theory provides results in less than 0.2 minutes for a rotor trim case shown in Figure 7. A single blade dynamics loop for a rigid wake model, taking into account a wake of 3 rotor revolutions, takes about 1 minute of computing time. Free-wake analysis using only 5 trailing vortices and calculating a single blade dynamics loop uses about 2 to 20 minutes of computer time for $\mu = 0.3$ and 0.1 respectively. The semi-empirical model provides results for a rotor trim loop in about 1 to 0.2 minutes between hover and $\mu = 0.3$. However, computing time for hover is given for a disturbed flight and the value for an ideal hovering flight case is equal to the time for $\mu = 0.3$. Therefore in the low speed region, computing time for a rotor trim loop using the semi-empirical model is nearly equal to the time needed by the vortex model for a single blade dynamics loop. For high speed flight, computing times for the semi-empirical model and the local momentum theory are nearly equal. Further reductions of calculation costs for the semi-empirical model may be attainable by refinement of the numerical calculation procedure.

Calculated blade loads versus radius and azimuth-angle for hovering and transition flight of the S 58, are shown in Figures 9 to 11 and compared with measurements (Reference 21). Results are presented versus radius for azimuth angles ψ = 0, 90, 180 and 270 deg. and versus azimuth angle for radial stations r = 0.95 and 0.85. For the hovering case, see Figure 9, the local momentum model cannot reproduce the important wake-contraction effects near the blade tips, whereas the results from the semi-empirical model and from the prescribed-contracted-wake analysis are almost identical and agreement with measurements is very good considering the difficulty in finding undisturbed hovering flights.

For the transitional advance ratio of μ = 0.064, blade loads are shown in Figure 10. At the advancing and retreating blade, the tip loading is increased by the tip vortices, whereas in the fore-aft position, blade loading is rather triangular. Plots of load versus azimuth also show typical tip vortex - blade interaction effects for the semi-empirical model and the prescribed-contracted-wake analysis, whereas the local momentum theory provides only average values. In spite of the fact that the semi-empirical model may overestimate the tip vortex effects for some azimuth angles, agreement with measurements is as good as for the prescribed-contracted-wake analysis.

Blade loads for the moderate advance ratio μ = 0.112 are presented in Figure 11. Again the typical blade tip loading effects owing to the tip vortices at the advancing and retreating blade can be noticed. Results of the semi-empirical model in general are similar to those of prescribed-contracted-wake analysis. The yields of 20 minutes of computing time invested in a free-wake model are also shown in Figure 11. In spite of the sophisticated model, the results are rather poor compared to measurements and results of the more simple methods. This may be due to the rough discretization of the wake, using only 5 trailing vortices and 12 steps around the azimuth.

Trends of calculated and measured blade load harmonics for the S 58 at advance ratios of μ = 0.064, 0.112 and 0.229 are presented in Figure 12. For low and moderate μ, the higher harmonics are underestimated by the local momentum theory and to some extent also by the rigid-wake analysis. For a typical forward flight condition (μ = 0.229) the local momentum theory as well as the semi-empirical model and the rigid-wake analysis nearly give the same results showing an extremum for the second harmonic. The increasing and decreasing of the higher harmonics with increasing μ in the transition flight region can only be read from the results of the semi-empirical model.

Some typical results from rigid rotor flight mechanics are given in comparison to measurement in Figures 13 and 14. As shown in Figure 13 (Reference 22) the cyclic control moment and the phase angle versus rotor thrust in hovering flight can only be predicted using the local momentum theory (i.e. the basis for the semi-empirical model) instead of the simple momentum equation. The local momentum theory shows the typical decrease of cyclic pitch effectiveness and the increase of longitudinal/lateral coupling with decreasing rotor

thrust in hovering flight. Disregarding the longitudinal control angle, which in the first place is affected by horizontal tail effectiveness, the lateral control angle in transition flight is shown for the BO 105 in Figure 14. Typical lateral control angle versus forward flight speed is predicted by the semi-empirical model much better than by the local momentum theory.

Results from rotor vibration calculations in the transition flight region are presented in Figures 15 and 16. Rotor hub in-plane oscillatory forces for the BO 105 at advance ratios of $\mu = 0$ to $\mu = 0.268$ are shown in Figure 15. As the forces predicted by the local momentum theory increase steadily with increasing μ, the semi-empirical model shows oscillatory forces first increasing and then decreasing with progressing μ in the transition flight region. For hover and for forward flight at $\mu = 0.268$, the results from both theories are nearly identical. Comparison with measurement (Reference 25) is made for the rotorhub inplane oscillatory moments of the BO 105 in transition flight in Figure 16. The semi-empirical model again shows the increase and decrease of the moments versus μ. As the local momentum theory underestimates the moments for small advance ratios, the agreement of the results predicted by the semi-empirical model with measurements is acceptable with regard to the amplitude and phase of the moments.

An example of rotor noise calculation is given in Figure 17 for the BO 105 during partial power descent (Reference 23). The plots of the calculated blade loads for several radial stations versus azimuth-angle show typical tip vortex - blade interaction effects at the advancing and retreating blade. Using the calculated aerodynamic blade loads as input data, the sound pressure can be estimated (Reference 24). The plots of calculated and measured sound pressure versus time show acceptable agreement, neglecting the extreme pressure peaks in the measurement which result from main rotor - tail rotor interference that is not included in the analysis. Predicted and measured sound pressure levels versus frequency, also coincide very well up to a frequency of about 375 Hz, which corresponds approximately to the 12th blade harmonic. Higher harmonics may be predicted correctly using smaller azimuthwise steps in the blade load calculations.

5. CONCLUSIONS

Treating the rotor as an integrated aerodynamic/dynamic system in standard rotor calculations, the induced velocities in the rotor disc have to be calculated accurately, especially when they are not small compared with the free stream velocity. Typical flight cases are hover and transition flight as well as flare and descent, when the wake is near to the rotor.

Rotor downwash analysis in standard calculations today is based either on momentum theory or on vortex-wake models. Typical momentum models, such as the local momentum analysis, can predict induced velocities accurately and reasonably in undisturbed hovering flight (neglecting wake contraction) and in all cases when the wake is far from the rotor, i.e. $\mu > 0.15$ at nose-down angles of the rotor disc. For all other cases when the wake is near to the rotor, vortex models, such as an empirical-prescribed-wake model or free-wake analysis, have to be consulted. Typical prescribed-wake models, using an experimental wake geometry taken from hovering flight, may also be applied to the transition flight region if the geometry is distorted according to the free stream velocity and computing time is tolerable for use in special cases. However, computing time for free-wake models, in transition flight cases, is too formidable to use these models in standard rotor calculations.

A semi-empirical downwash model which combines momentum theory with the properties of a vortex-wake model, may be an efficient tool for standard rotor calculations both in terms of computing time and accuracy. Local momentum theory can be extended to simulate wake contraction and tip losses in order to give nearly the same results in hovering flight as an experimental-prescribed-wake model. A special super-positioning principle can also simulate tip vortex - blade interactions and other effects known from vortex models and experiments in the transition flight region. Therefore, results of the fast semi-empirical downwash model are very similar to those calculated by much more expensive vortex-wake analysis.

The usefulness of the semi-empirical downwash model in standard rotor calculations, in order to predict rotor performance, structural limitations, vibrations and acoustics, can be demonstrated by predicting, e.g. blade loads, rotor hub inplane oscillatory stresses and rotor noise, with acceptable accuracy for flight cases where results from local momentum theory are inadequate.

6. REFERENCES

1) H. Glauert, A General Theory of the Autogyro, Aeronautical Research Council (Great Britain), R&M No. 1111, (1926)

2) H. Glauert, On the Vertical Ascent of a Helicopter, Aeronautical Research Council (Great Britain), R&M No. 1132, (1927)

3) S. Goldstein, On the Vortex Theory of Screw Propellers, Royal Society Proceedings, Ser. A 123, (1929)

4) K.W. Mangler and H.B. Squire, The Induced Velocity Field of a Rotor, Aeronautical Research Council (Great Britain), R&M No. 2642, (1953)

5) R.A. Ormiston, An Actuator Disc Theory for Rotor Wake Induced Velocities, AGARD-CPP-111, (1972)

6) E.R. Wood and M.E. Hermes, Rotor Induced Velocities in Forward Flight by Momentum Theory, AIAA/AHS VTOL Research, Design, and Operations Meeting, AIAA Paper No. 69-244, (1969)

7) H.H. Heyson and S. Katzoff, Induced Velocities Near a Lifting Rotor with Nonuniform Disc Loading, NACA TR 1319, (1957)

8) M.A.P. Willmer, The Loading of Helicopter Rotor Blades in Forward Flight, Aeronautical Research Council (Great Britain), R&M No. 3318, (1963)

9) R.A. Piziali and F.A. DuWaldt, Computation of Rotary Wing Harmonic Airloads and Comparison With Experimental Results, Proceedings 18th Annual Forum, American Helicopter Society, (1962)

10) M.P. Scully, Approximate Solutions for Computing Helicopter Harmonic Airloads, Massachusetts Institute of Technology, TR 123-2, (1965)

11) G. Daske, I.A. Simons, Rotorberechnung mit Berücksichtigung der ungleichförmigen Verteilung der induzierten Geschwindigkeiten, MBB-Report DF 70, (1967)

12) R.A. Piziali, Method for the Solution of the Aeroelastic Response Problem for Rotating Wings, Jl. Sound and Vibration, Vol. 4, No. 3, (1966)

13) T.T. Theodorsen, Theory of Static Propellers and Helicopter Rotors, 25th Annual Forum, American Helicopter Society, No. 326, (1969)

14) M. Jogelar and R. Loewy, An Actuator-Disc Analysis of Helicopter Wake Geometry and the Corresponding Blade Response, USAAVLABS Technical Report 69-66, (1970)

15) A.J. Landgrebe, An Analytical and Experimental Investigation of Helicopter Rotor Hover Performance and Wake Geometry Characteristics, USAAMRDL Technical Report 71-24, Eustis Directorate, U.S. Army Air Mobility Research and Development

16) R. Stricker, W. Gradl, G. Polz, Aerodynamische Arbeitsgrundlagen für zukünftige Hubschrauberentwicklungen, MBB-Report UD-159-75, (1975)

17) A.J. Landgrebe, An Analytical Method for Predicting Rotor Wake Geometry, Jl. American Helicopter Society, Vol. 14, No. 4, (1969)

18) S.G. Sadler, Development and Application of a method for predicting rotor free wake positions and resulting rotor blade air loads, NASA CR-1911, (1971)

19) P.J. Carpenter, B. Fridovich, Effect of a Rapid Blade-Pitch Increase on the Thrust and Induced Velocity Response of a Full-Scale Helicopter Rotor, NACA TN 3044, (1953)

20) A.R.S. Bramwell, Helicopter Dynamics, Edward Arnold, London, (1976)

21) J. Scheiman, A Tabulation of Helicopter Rotor-Blade Differential Pressures, Stresses, and Motions as Measured in Flight, NASA TM X-952, (1964)

22) H. Huber, V. Langenbucher, H.J. Dahl, E. Laudien, Theoretische Grundlagen und Untersuchungen zur Flugmechanik von Drehflüglern, MBB-Report UD-131-74, (1974)

23) E. Laudien, Untersuchungen zur Lärmminderung an Hubschraubern, MBB-Report UD-197-76, (1976)

24) K. Heinig, Untersuchungen zur Lärmminderung bei Hubschraubern, MBB-Report TNA D12-28/70, (1970)

25) G. Stiller, Analyse der BO 105 - Getriebevibrationen im Hinblick auf Schwingungsisolationsmaßnahmen, MBB-Report TN-DE 132-12/77, (1977)

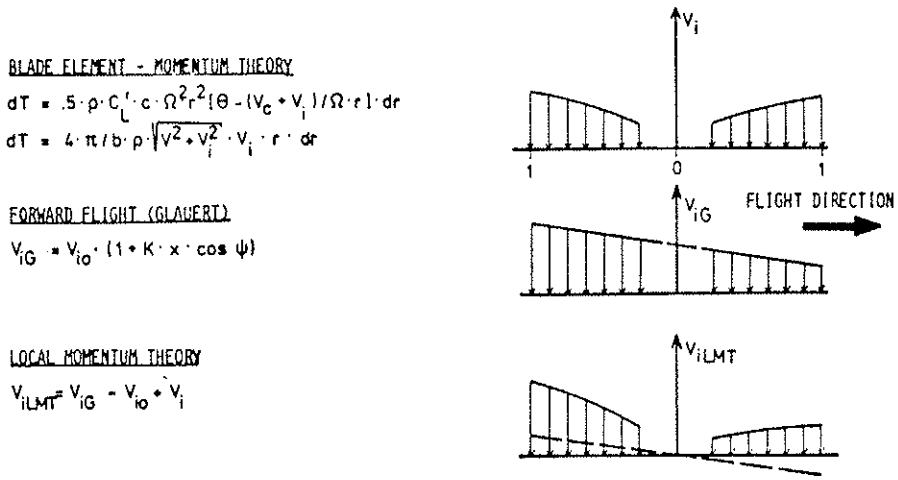

Figure 1: Principle of local momentum theory

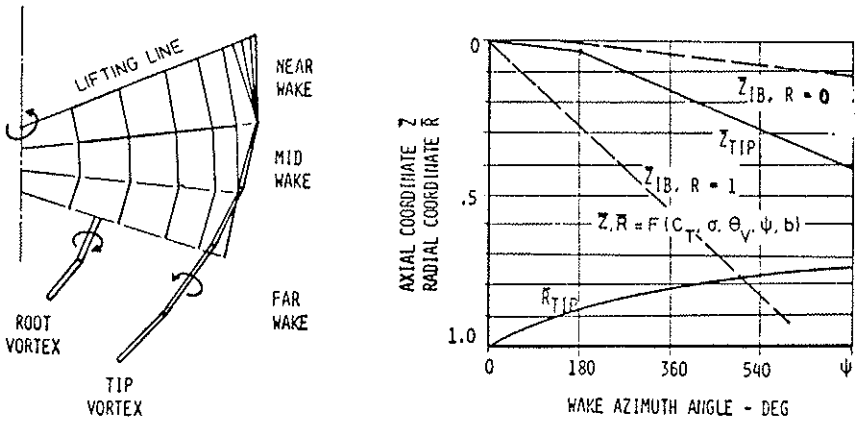

Figure 2: Wake structure and geometry of Landgrebe for the prescribed-contracted-wake model 'UNDUFL'

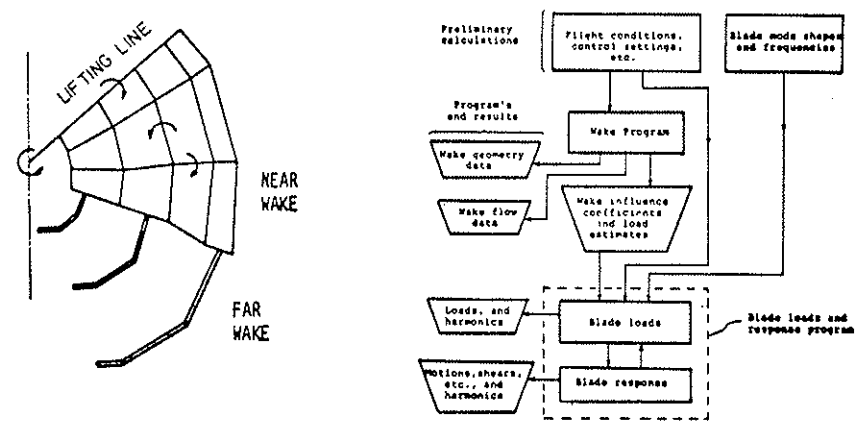

Figure 3: Wake structure and program flow diagram for the free - wake model of Sadler

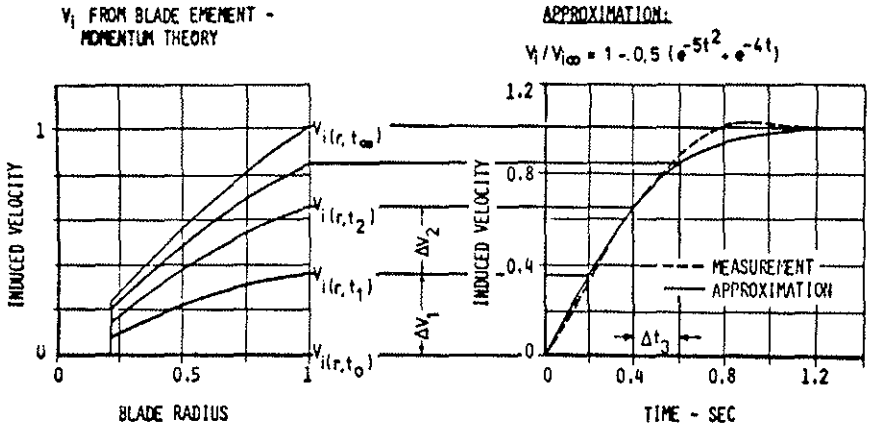

Figure 4: Hovering flight

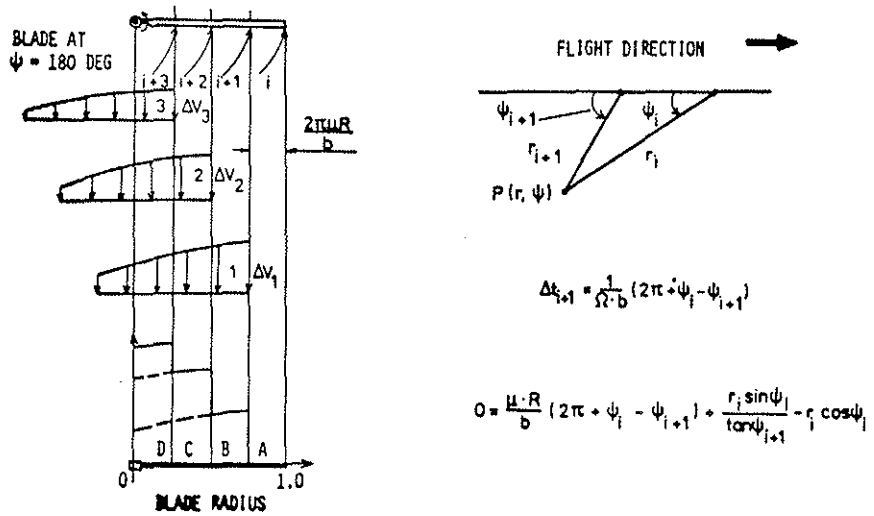

Figure 5: Forward flight

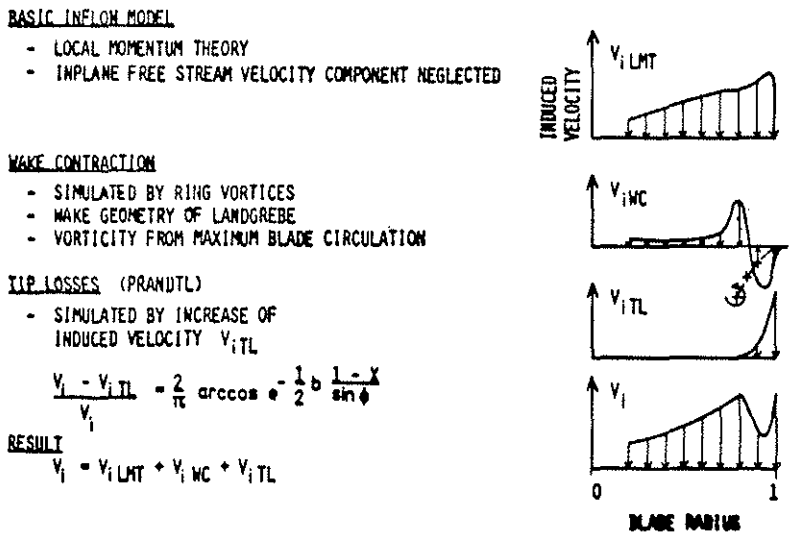

Figure 6: Wake contraction and tip loss consideration

Figure 4 to 6: Principle of the semi-empirical downwash model

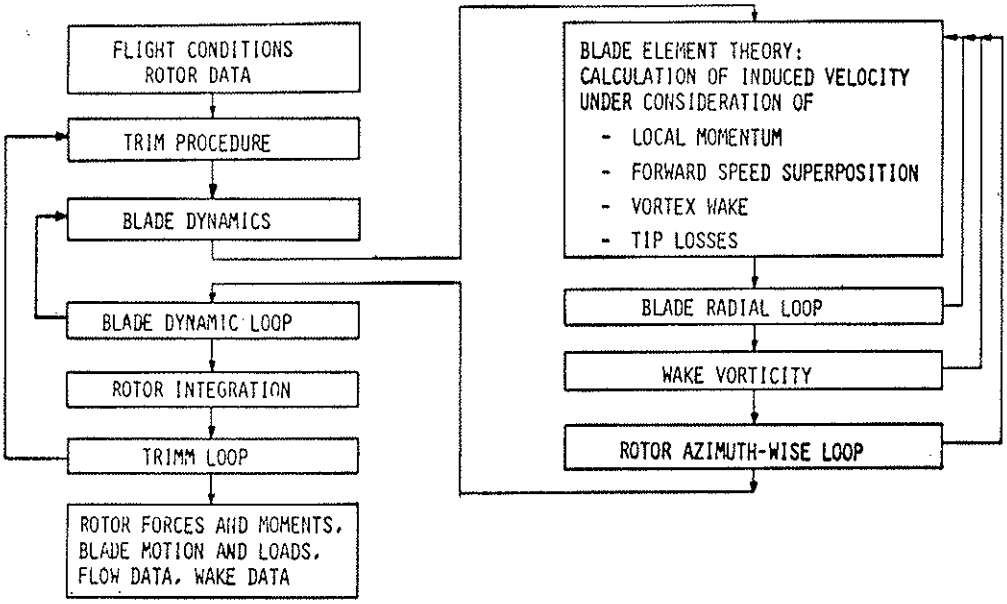

Figure 7: Rotor calculation block diagram using the semi - empirical downwash model

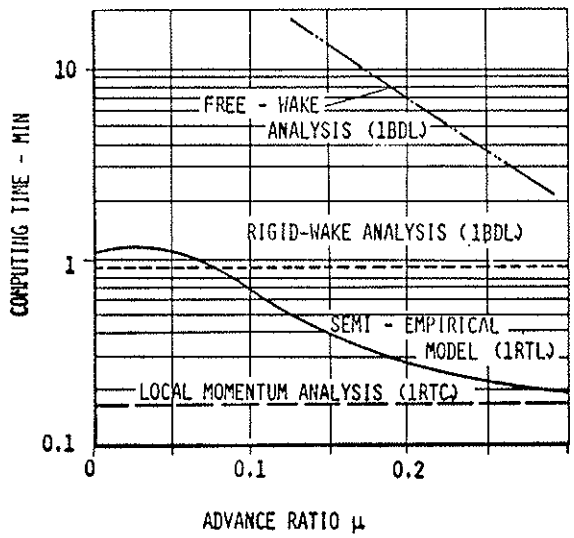

Figure 8: Computing time vs. advance ratio for selected downwash models

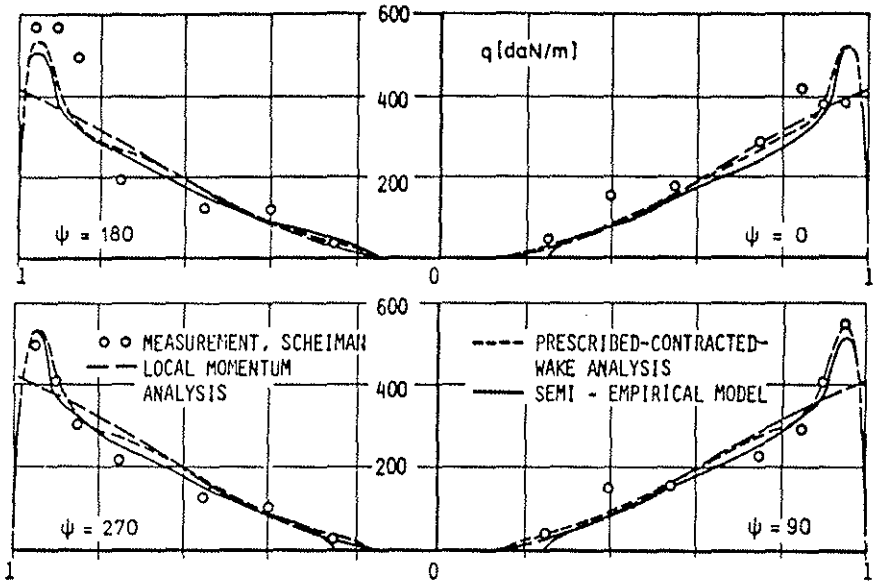

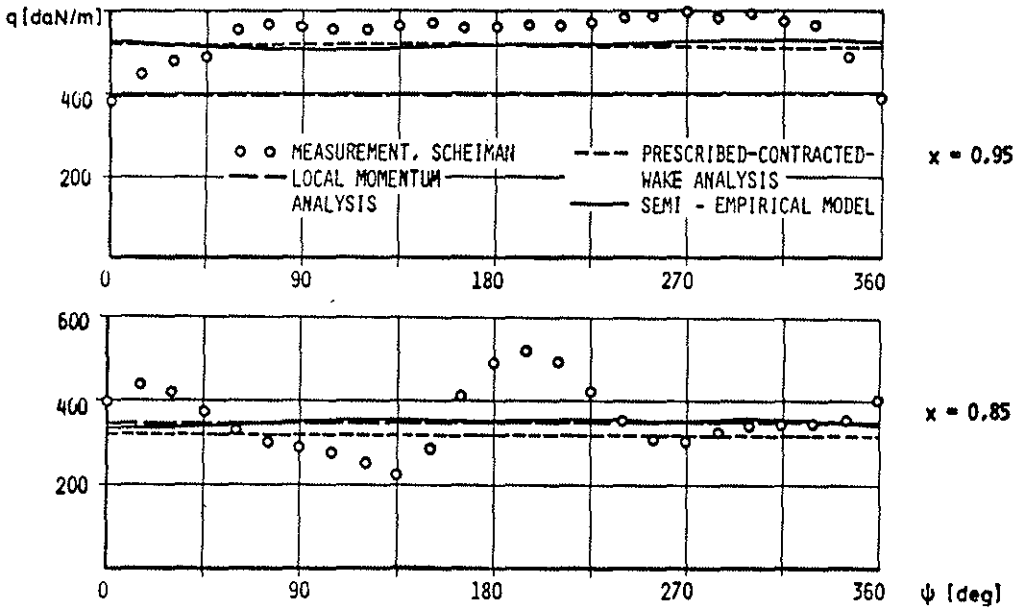

Figure 9: Blade loads vs. radius and azimuth-angle for the S58, m = 5240 kg, μ = o

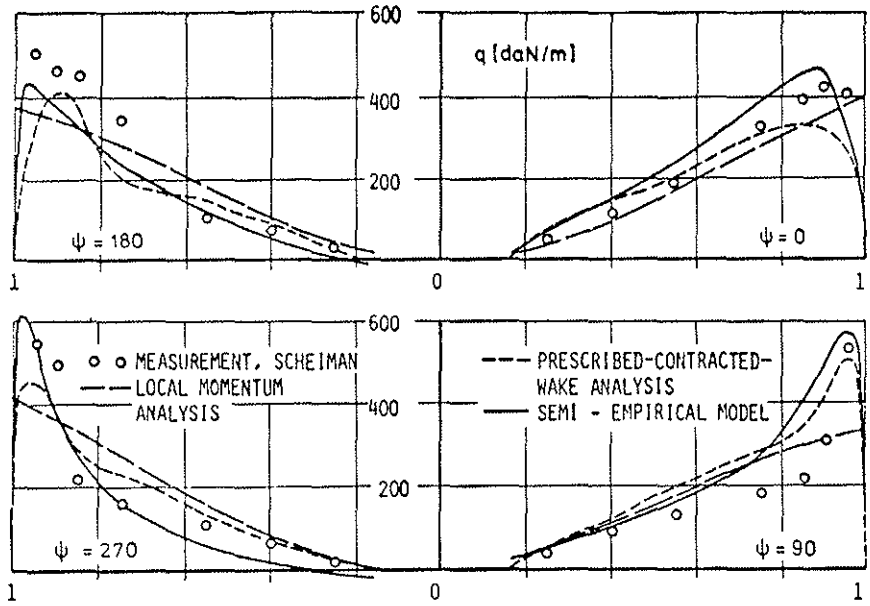

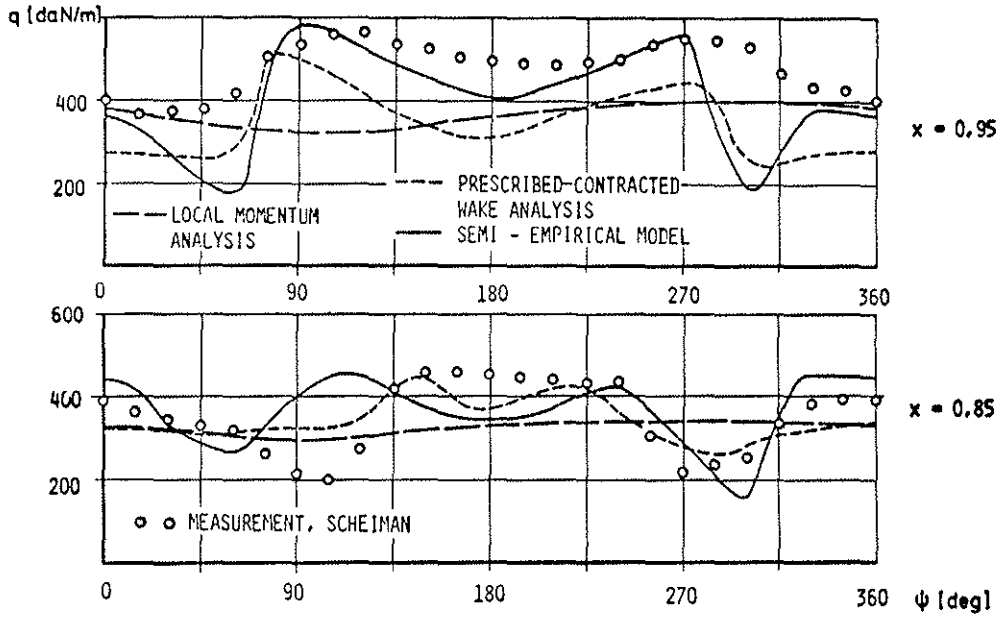

Figure 10: Blade loads vs. radius and azimuth-angle for the S58, m = 5140 kg, μ = 0.064

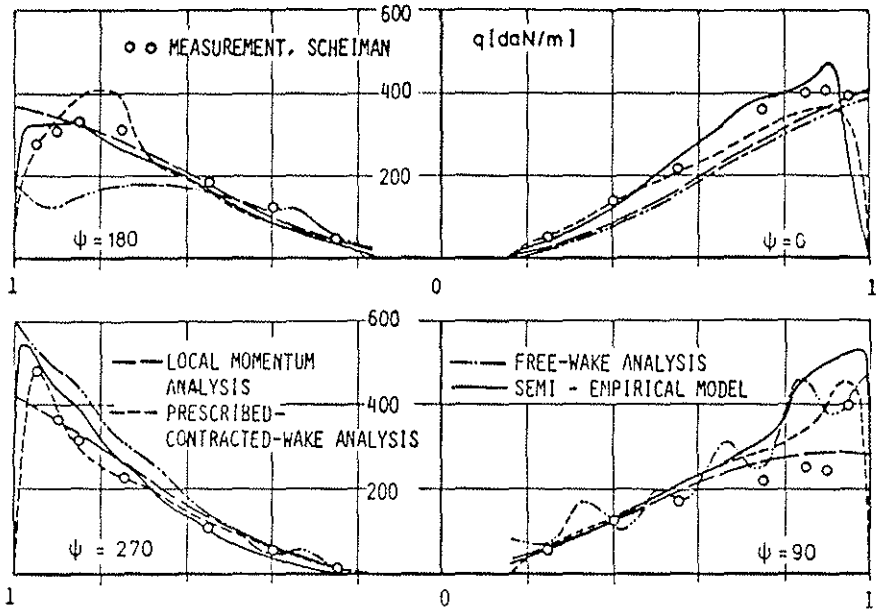

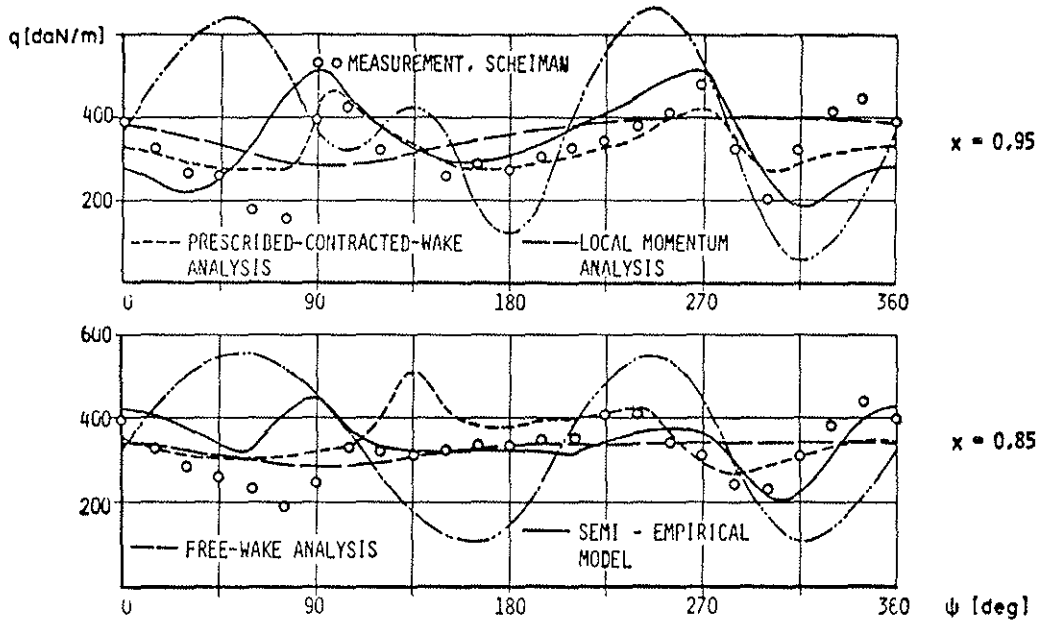

Figure 11: Blade loads vs. radius and azimuth-angle for the S58, m = 5180 kg, μ = 0.112

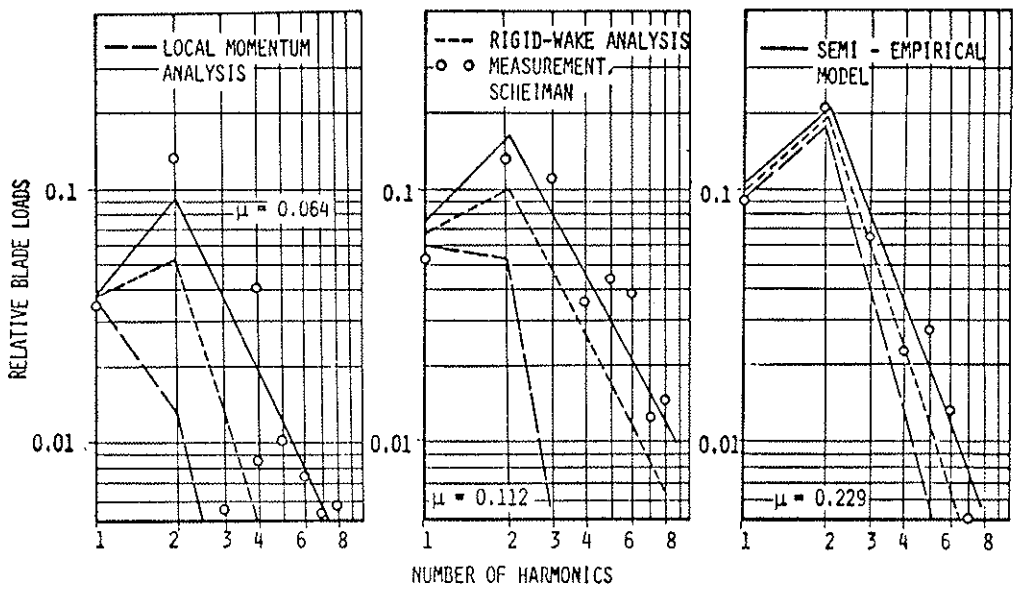

Figure 12: Trends of blade load harmonics for the S58 at μ = 0.064, 0.112, and 0.229

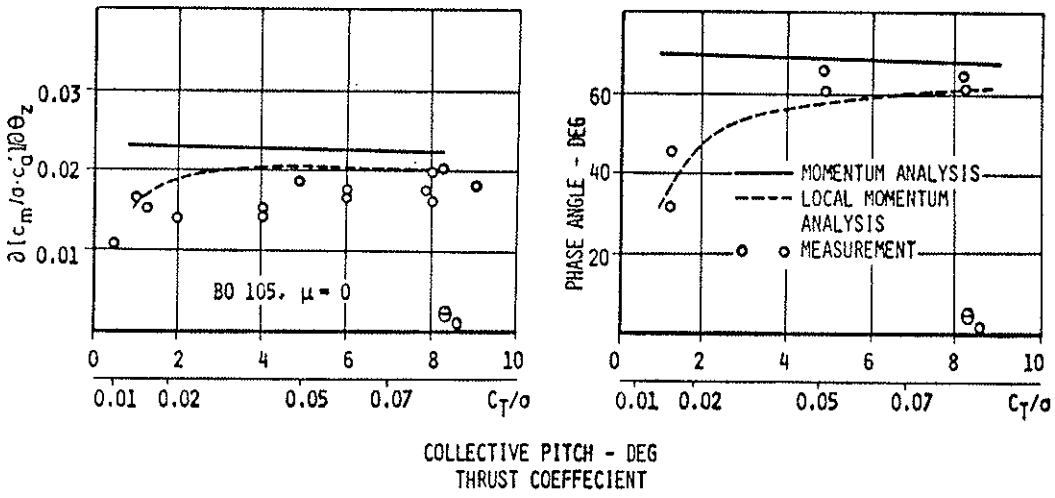

Figure 13: Cyclic control moment and phase angle for BO 105 at hover

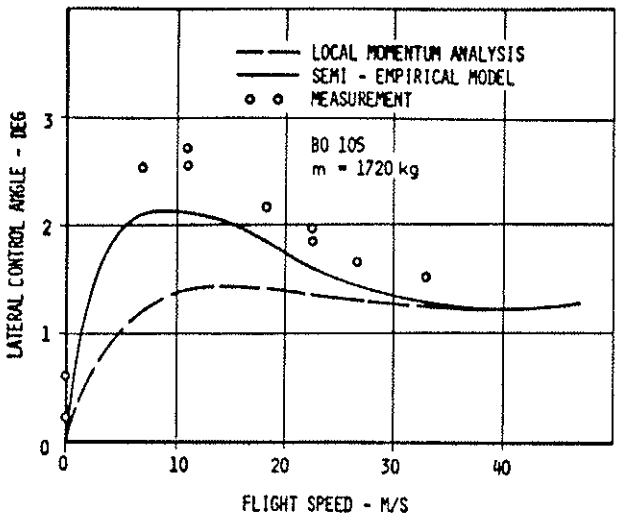

Figure 14: Lateral control angle in transition flight for the BO 105

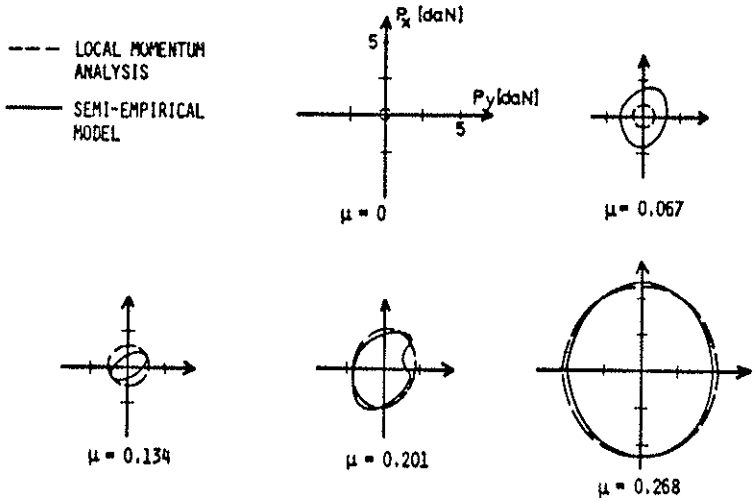

Figure 15: Rotorhub inplane oscillatory forces vs. μ for the BO 105, m = 1720 kg

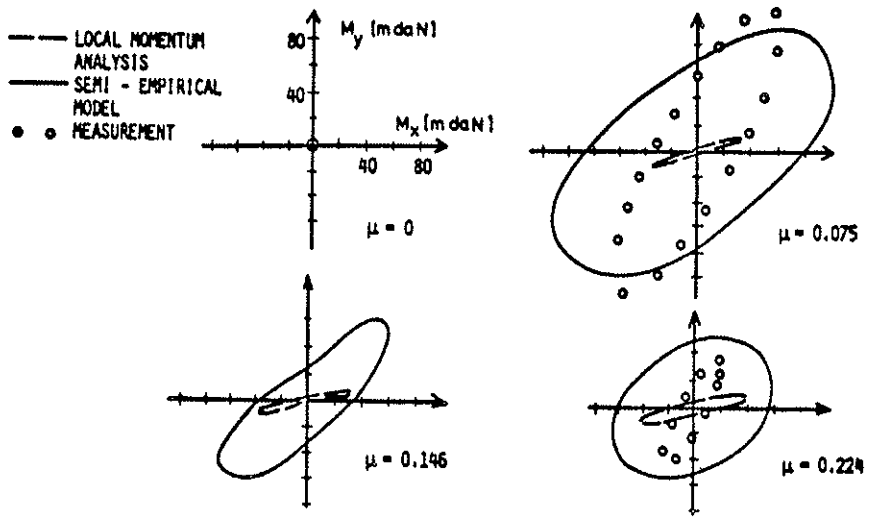

Figure 16: Rotorhub inplane oscillatory moments vs. μ for the BO 105, m = 2000 kg

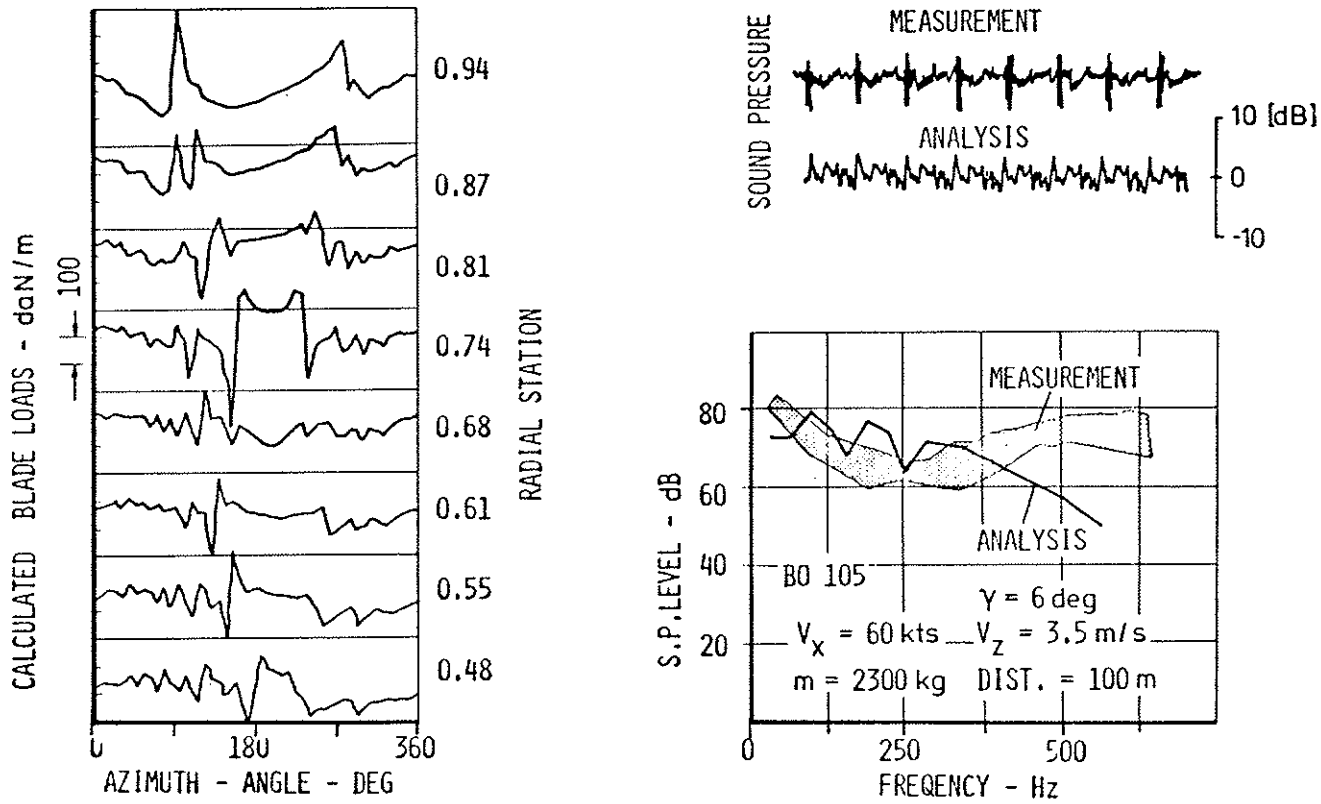

Figure 17: Rotor noise of BO 105 during partial power descent